MEE05:30

Through-wall imaging using a hand-held UWB SAR system

Alexander Rajula

This thesis is presented as part of Degree of
Master of Science in Electrical Engineering

Blekinge Institute of Technology
Juni 2012

Blekinge Institute of Technology
School of Engineering
Department of Applied Signal Processing
Supervisor: Dr. Mats Pettersson
Examiner: Dr. Mats Pettersson

Abstract

Synthetic aperture radar systems are used extensively for imaging vast areas using electromagnetic radiation. Radar systems have the benefit of being able to image areas which optical light cannot penetrate, and makes radar suitable for surveillance and weather monitoring, or monitoring through difficult atmospheric conditions. This thesis investigates whether a hand-held radar can function as a synthetic aperture radar device, by employing standard synthetic aperture radar projection and filtering algorithms, and whether it is possible to image contents within walls with the same equipment.

Acknowledgements

I wish to thank three, albeit now deceased, great poets. Carl Sagan, for his effort to increase scientific awareness in the public mind, Richard Feynman for his enthusiastic and engaging descriptions of the natural world, whom I would have much to owe had he been alive. Last but not least, I thank Gene Roddenberry for instigating a televisio-cinematic revolution and inspiring numerous young people to pursue scientific and engineering careers.

I also wholeheartedly thank Mats Pettersson, Viet Thuy Vu and Thomas Sjögren for their support and laying the foundations on which much of this thesis is based.

A nod goes out to David Erman and Wlodek Kulesza whose courses greatly improved my academic writing skills.

I thank Dan Axelsson at Cinside AB for this interesting topic, and the ease with which we worked together on this project

Beam me up Scotty!

Contents

List of Figures

List of Tables

1 Introduction

Radio detection and ranging (RADAR) is a system used to extract useful information from reflected electromagnetic signals. Radar has been in use since the early 1900s, first described in a patent by Hülsmeyer under the description *telemobiloscope* [8]. Radar as we know it today developed from the 1920s and onwards, and gained a substantial momentum during World War II [7]. It has since then been employed extensively in a variety of fields, for instance weather forecasting [9], imaging of objects in space [3] and more recently to generate 2D human-readable images of ground surfaces, for instance damage assessment in forests [6].

The basic operation of any radar system is a signal generator, an amplifier, an antenna for transmission of radar pinging signals, an antenna for receiving radar echoes, and the necessary analog or digital signal processing apparatus to extract useful information from the radar echoes. The exact details of the various components depend on the application of the radar system. Since the applications are so diverse, there are also a wide range of radar systems in use today. The most basic building blocks are outlined in Fig. 1.

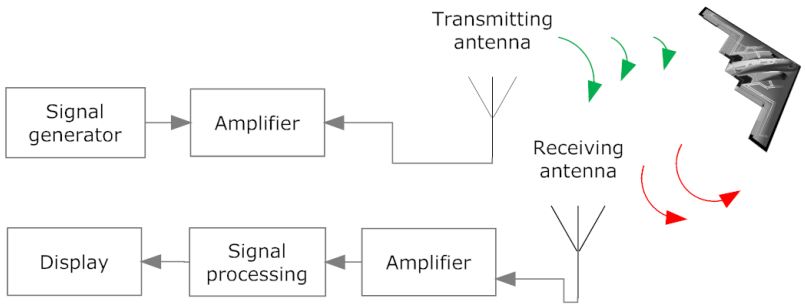

Figure 1: Rudimentary radar system

1.1 Introducing synthetic aperture radar systems

Normally, a radar can only capture reflections within its antenna beamwidth range, which limits the area any stationary radar can image. Synthetic aperture radar (SAR) systems extend this area by employing single (monostatic) or dual (bistatic) antennas in combination with a moving platform, usually an aeroplane, to capture reflections from a vast area [15].
In a SAR system, the kind of radar ping (waveform) and its pulse repetition frequency (PRF) are important, since they determine the resolution in range. Simply put, finer range resolution means that smaller objects can be discerned in the final SAR image.

1.2 A typical SAR system

Any SAR system employs a specific waveform with a certain PRF. The reflected complex signal (amplitude and phase) is recorded over the entire synthetic aperture for real-time or post processing. This is the raw received data. The raw data is then processed by *pulse compression* to increase range resolution and signal-to-noise ratio (SNR). The pulse-compressed data may then be processed by a radio-frequency (RF) interference (RFI) filter which aims to cancel out interference due to non-radar sources, for instance television broadcasts [19]. Once the data has been appropriately compressed and filtered, a SAR imaging algorithm is employed to create a 2D human-readable image from the radar data. There are various SAR imaging algorithms in use, operating either in the time or frequency domains. The selection of which imaging algorithm to use depends on image quality requirements just as much as the requirement in processing speed. Studies have been made comparing the complexity between time domain and frequency domain algorithms, as well as comparisons between different time and frequency domain algorithms to asses computational complexity and image quality [2][16][17].
As a last step, a filtering process known as *apodization* is typically employed to decrease frequency-domain sidelobe levels [12]. The SAR system described is depicted in Fig. 2.

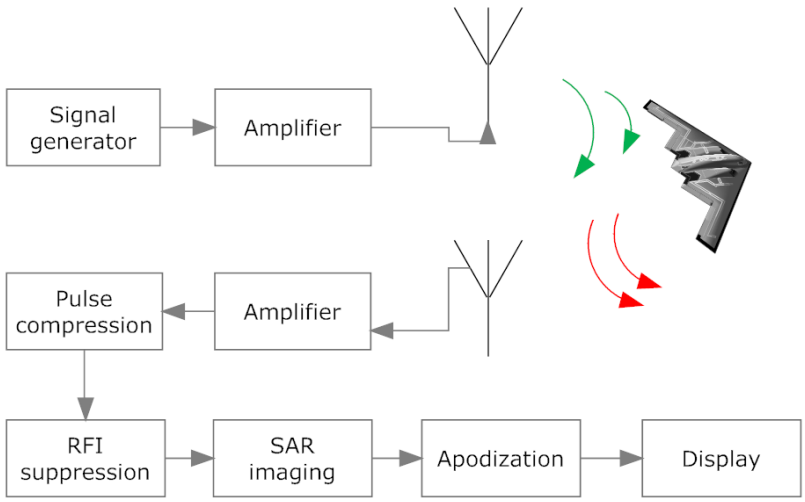

Figure 2: Typical SAR system

1.3 Problem statement

This thesis tries to solve the problem of imaging the contents within a wall or other solid object using a SAR system. There is, however, one main difference between the problem faced in this thesis and a typical SAR system, in that the

radar will operate in relatively close range to the object being probed, and in addition the radar will be scanned by hand, not by an aeroplane.

1.4 Thesis scope

The scope of this thesis is to implement SAR imaging algorithms and necessary pre- and postprocessing steps, verify the functionality of the algorithms and use the algorithms to process hand-held radar data. The end product is a SAR model and processor implemented in Scilab [11] and the C programming language, which can be used to simulate and process hand-held radar data to generate a 2D human-readable image. In addition, the thesis covers parameter requirements for hand-held SAR imaging to work, and presents an analysis on how nonlinear scanning may be handled.

1.5 Thesis outline

This chapter has given a basic description of radar systems in general, and SAR systems in particular. In the following chapter I give a more detailed technical description of SAR systems. In chapter four the Scilab model is descibed in detail, as well as a description of the radar equipment used to gather data. Chapter four also contains a subchapter on verification of the system model.

1.6 Research questions

There are a number of concrete research questions associated with this topic, some of which are:

- What waveforms are most suitable, or are we constrained by the radar equipment?
- Is Global Backprojection applicable for imaging the radar data or do we need another imaging algorithm?
- What PRF values are most optimal?
- Do we need RFI suppression?
- Do we need to employ apodization?

1.7 Methodology

The methodology in this thesis is simulation using Scilab and a C program guided by standard radar equations and SAR equations in particular regarding range resolution and image quality.

2 Background and related work

This chapter presents a detailed report on the key characteristics of SAR systems, and concludes by a review on research related to this thesis.
In a SAR system, several subsystems, equations and parameters are of importance for design and evaluation. Some of them are described below, in processing order.

2.1 The radar range equation

Most crucial to all radar designs is the radar range equation, which relates the transmitted and received signal powers:

$$P_r = \frac{P_t G_t}{4\pi R^2} \frac{\sigma A_e}{4\pi R^2} \tag{1}$$

The equation is a product of two parts, the signal energy at the scattering object, and the received signal energy at the radar equipment. Here, P_t is the transmitted radar energy, G_t is the gain of the transmitting antenna, R is the distance to the object scattering the energy, σ is the radar cross section of the scattering object, and A_e is the aperture size of the receiving antenna. The squared magnitude of the distance and the factor of 4π accounts for the spherical propagation of the energy of an isotropic radiator.
Given this equation, it is possible to estimate either the radar cross section of an object, or it can be used to evaluate power and antenna parameters for a particular design.

There is also a relation between effective antenna aperture area and antenna gain, which is useful if the same antenna is used for both transmission and reception:

$$G_t = \frac{4\pi A_e}{\lambda^2} \tag{2}$$

Here, λ is the wavelength of the signal transmitted.

In addition a standard expression for the minimum received signal level is used, which is dependent on the required signal-to-noise ratio:

$$S_{min} = kT_o BF_n(S/N) \tag{3}$$

Here, the first three parameters, kT_0B, is the thermal noise from an ideal ohmic conductor. k is Boltzmann's constant and T_0 is the temperature at about 20 centigrade (290K) [14]. B is the bandwidth of the signal, F_n is the receiver noise figure, and S/N is the required signal-to-noise ratio. This equation is valid for one radar pulse, but in most radar systems used today, several pulses are integrated to increase the probability of correct detection. The required received signal energy per pulse is thus *less*, which is usually incorporated by a factor of $nE_i(n)$, where n is the number of pulses added, and $E_i(n)$ is the efficiency of

adding them together.
The resulting expression is thus:

$$S_{min} = \frac{kT_oBF_n(S/N)}{nE_i(n)} \tag{4}$$

2.2 Signal waveforms

The most simple waveform used in radar is a continuous wave, in which the doppler shift is used to detect moving targets. This is unsuitable for UWB SAR systems, and instead a chirp signal is employed, in which the signal frequency increases linearly in time during pulse transmission. A typical chirp signal is mathematically described by [13]:

$$s_t(\tau) = e^{-i2\pi(\phi_0 + f_c\tau + k\tau^2)}, \tau \in \left[-\frac{T_p}{2}, \frac{T_p}{2}\right] \tag{5}$$

Here, τ is the time over which the pulse is active, ϕ_0 is the phase, k is the chirp rate, f_c is the center frequency of the signal and T_p is the total pulse length. Fig. 3 shows an example chirp waveform. The center frequency is set to 200MHz with a chirp rate of $100 * 10^6$ and signal duration of one millisecond.

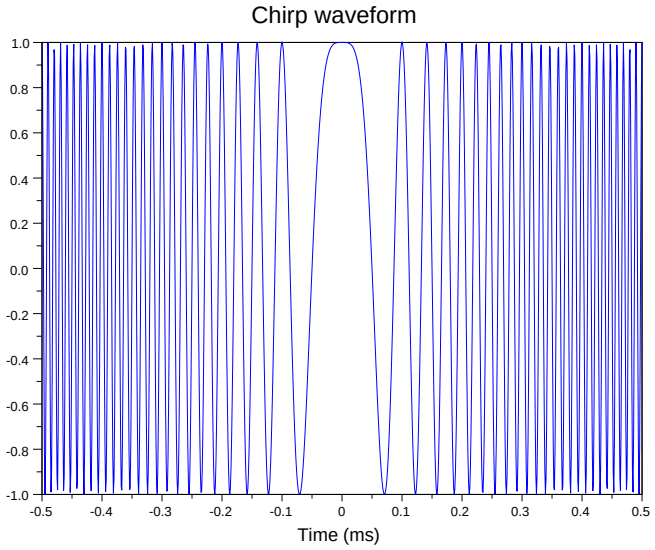

Figure 3: Typical chirp waveform

2.3 Azimuth doppler effects

Since the SAR system moves with a velocity v_{sar} with respect to ground objects, the received radar echo will be subject to a frequency shift according to the well known doppler equation:

$$f = \left(\frac{c + v_{sar}}{c + v_s} \right) f_0 \tag{6}$$

Here, v_s is the velocity of a ground object. For stationary ground objects, the shift simplifies to:

$$f = \left(1 + \frac{v_{sar}}{c} \right) \tag{7}$$

In the normal SAR case, the platform may move with great velocity, and echoes from different azimuth positions will be collected at the same time, each echo having a different frequency shift. When the platform moves with high velocity, this effect must be accounted for.
For the case of hand-held radar equipment, radar velocities will not exceed one meter per second, and so the fractional frequency shift will be insignificant, which directly tells us that we will not need to consider azimuth doppler shifts in this thesis.

2.4 Time-bandwidth product effects

When digitally creating the chirp signal, it is important to keep several factors in mind, in particular sampling time and signal duration. The chirp rate and the bandwidth of the signal are related by:

$$B = k * t_{end} \tag{8}$$

Here, k is the chirp rate and t_{end} is the signal duration. There are two variables to control here to make the chirp signal reach the full spectral content. We now introduce the time-bandwidth product (TBP), which typically is a constant, and measures the granularity of the chirp spectrum. Since the chirp signal is digitally created with a certain number of samples, undersampling misses spectral components. Using the TBP to control both end time and chirp rate is a simple way of generating a chirp signal of desired spectral quality. A higher TBP means that more spectral components will be captured by the digital signal. A lower TBP means that more spectral components will be missed. The selection of TBP for simulation purposes is a tradeoff between signal quality and processing time, since increasing the time of the signal will also lead to more waveform samples.
In the figures below, the spectrum of a chirp signal with different values for TBP are plotted to illustrate the effects TBP has on the signal.

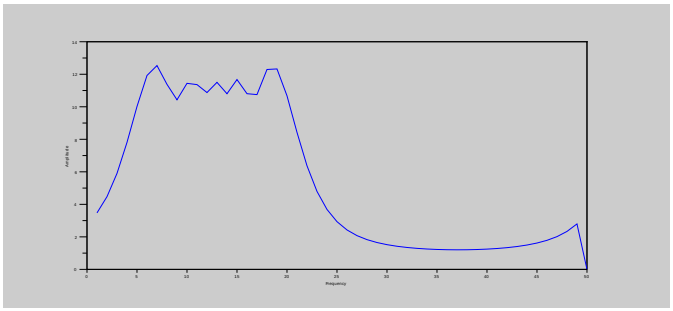

Figure 4: Chirp signal spectrum with TBP of 10.

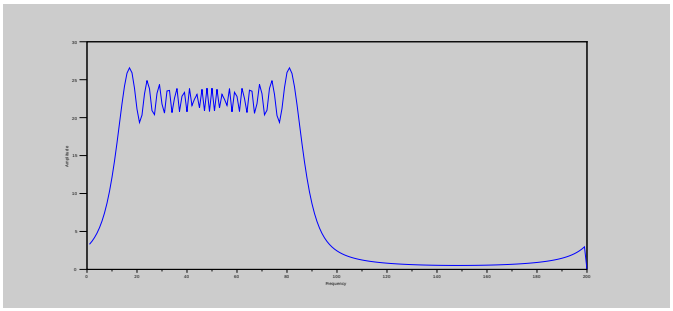

Figure 5: Chirp signal spectrum with TBP of 40.

2.5 Pulse compression

Pulse compression is a signal processing technique to increase range resolution and signal to noise ratio. It works by convolving the received signal with a time-reversed and conjugated version of the transmitted signal. This is nothing else than computing the cross-correlation of the two signals, also known as matched filtering. The received signal will be attenuated and arrive at a time offset with respect to the transmitted signal. If we disregard the attenuation, the received signal can be described by [13]:

$$s_r(\tau) = e^{-i2\pi\left(\phi_0 + f_c\left(\tau - \frac{2R}{c}\right) + k\left(\tau - \frac{2R}{c}\right)^2\right)}, \tau \in \left[-\frac{T_p}{2} + \tau_d, \frac{T_p}{2} + \tau_d\right] \tag{9}$$

The pulse-compressed signal is thus computed as follows:

$$s_{pc}(\tau) = s_r(\tau) * s_t(-\tau)^* \tag{10}$$

The convolution is easily computed in the frequency domain by first utilizing the Fourier transform, typically with the FFT algorithm. A pulse-compressed chirp signal is shown in Fig. 4.

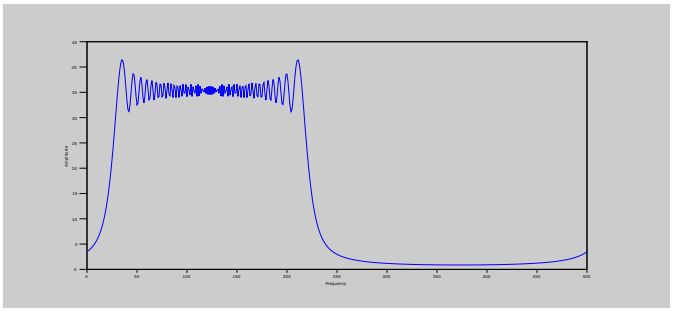

Figure 6: Chirp signal spectrum with TBP of 100.

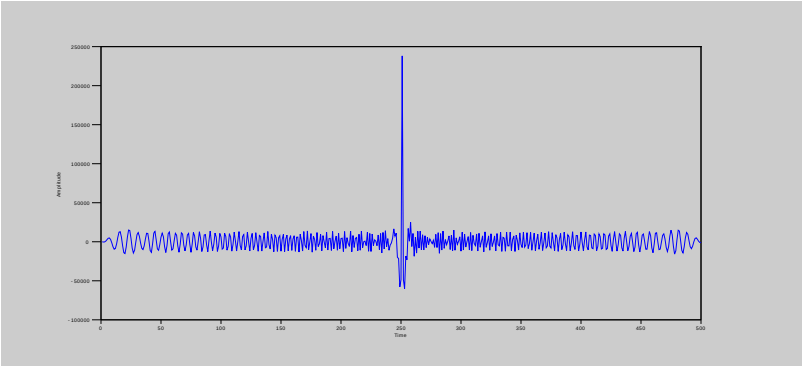

Figure 7: Pulse-compressed chirp signal with TBP of 100.

2.6 Pulse repetition frequency and resolution

Since a SAR system images a two-dimensional surface, there are relationships between antenna beamwidth θ_B, pulse repetition frequency PRF, pulse bandwidth B, platform speed v_p, range distance R, aperture length L_{sa} and the *range* δ_r and *crossrange* δ_{cr} (also known as *azimuth*) resolutions.
For a real aperture, the approximation $\theta_B \approx \frac{\lambda}{D}$ is used which gives a linear crossrange resolution of:

$$\delta_{cr} = \frac{R\lambda}{D} \tag{11}$$

Here, D is the aperture diameter.
For a synthetic aperture, we have the advantage that we can form extremely large apertures by physically moving the radar. Let us assume that the platform moves in a straight line perpendicular to the scene being observed. The length of the aperture is thus $L_{sa} = v_p * T$, where T is the time over which the aperture is formed. From the SAR, the scene rotates with an angular velocity of $\Omega = v_p/R$. The total angle through which the SAR rotates is thus $\Omega T = v_p T/R = \Delta\theta$. A stationary target appears to the SAR to have a line-of-sight velocity of Ωr, where

r is the crossrange distance of the target. This will result in doppler shifts of $2v_{target}/\lambda = 2\Omega r/\lambda$. If we assume that the frequency between successive returns of radar signals is $\Delta f = 1/T$, and combine this with the doppler frequency shift, we get the following crossrange resolution [14]:

$$\delta_{cr} \approx \frac{\Delta f}{f_{doppler}} = \frac{\lambda}{2\Omega T} \approx \frac{R\lambda}{2L_{sa}} \approx \frac{\lambda}{2\Delta\theta} \approx \frac{\lambda R}{2L_{sa}} \tag{12}$$

Here, $\Delta\theta$ is the synthetic aperture angle, as seen from the target.

An equation for range resolution is easily derived. Assume the signal to have a bandwidth B, which rougly gives a signal period of $\tau \approx \frac{1}{B}$. The signal needs to travel two ways, and since it travels at the speed of light, we get the following range resolution:

$$\delta_r \approx \frac{c}{2B} \tag{13}$$

Let us now see if we can derive the constraints for PRF. The derivation is based on [14], see Fig. 4. Imagine the scene illuminated by the radar beam at a particular slice of the total area covered, and also imagine two objects located at the ends of the beamwidth area illuminated. Name the objects A and B. For the SAR system, the apparent angular velocity is $\Omega = \frac{V}{R}$. The angle between the center of the radiation beam and the objects A and B is $\frac{\Theta_B}{2} \approx \frac{\lambda}{2D}$. The velocity of objects B and A is thus:

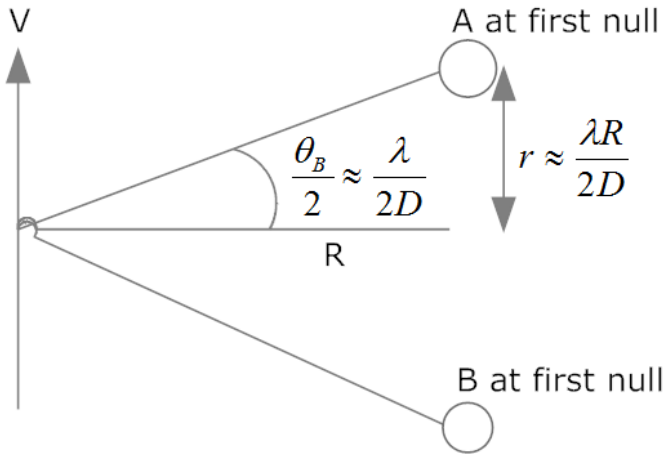

Figure 8: Illuminated area over the first-null beamwidth

$$\pm\,\Omega r \approx \pm\left(\frac{V}{R}\right)\left(\frac{\lambda R}{2D}\right) = \pm\frac{\lambda V}{2D} \tag{14}$$

The range of relative velocities over the area illuminated is thus:

$$\frac{\lambda V}{D} \tag{15}$$

This gives a range of doppler frequencies:

$$\Delta f_d = \frac{2}{\lambda}\frac{\lambda V}{D} = \frac{2V}{D} \tag{16}$$

If we want to avoid velocity ambiguity, this sets a constraint on the PRF:

$$f_{pr} \geq \frac{2V}{D} \tag{17}$$

However, we also want to avoid range ambiguity and eclipsing, i.e if we transmit pulses too fast, we will not be able to determine from which pulse an echo corresponds, which gives us:

$$f_{pr} \leq \frac{c}{2R} \tag{18}$$

Combining these two inequalities we get:

$$\frac{2V}{D} \leq f_{pr} < \frac{c}{2R} \tag{19}$$

For stripmap SAR, we can use the relation $\delta_{cr} = \frac{D}{2}$, which leads to:

$$\frac{V}{\delta_{cr}} \leq f_{pr} < \frac{c}{2R} \tag{20}$$

We see here that the crossrange resolution and the range are coupled, and can thus not be selected independently of each other:

$$\frac{R}{\delta_{cr}} \leq \frac{c}{2V} \tag{21}$$

According to [14], a more sophisticated expression is:

$$\frac{R}{\delta_{cr}} \leq \frac{c}{4.7V} \tag{22}$$

2.7 Radio frequency interference suppression

When working with low-frequency SAR, or radar systems in general, the received radar signal may contain energy from sources other than the radar transmitter. One possible source is television broadcasts, and if the radar is operated at frequencies in which it is known that other sources of radiation in the same frequency band are active, then radio frequency interference suppression filters may be needed to extract any useable radar data. If no RFI cancellation is employed, the radar signal may drown in background noise. Recently, an adaptive line enhancer in conjunction with the Normalized Least Mean Square (NLMS) algorithm has been proposed to act as the filter [18].
At the heart of the suppression system is the coefficient updating algorithm:

$$\mathbf{w}(n+1) = \mathbf{w}(n) + \frac{\beta}{\mathbf{x}^T(n)\mathbf{x}(n)}\mathbf{x}^*(n)\left[s(n) + v(n)\right] \tag{23}$$

Here, $\mathbf{w}$ is the filter coefficients, β is the filter convergence constant, $\mathbf{x}$ is the reference signal, and $s + v$ is the radar plus thermal noise signal.
The input to the ALE is a sum of terms:

$$d(n) = s(n) + v(n) + \rho(n) \tag{24}$$

Here, ρ is the RFI signal.
The reference signal $\mathbf{x}$ to the adaptive FIR filter is created by delaying the ALE input an integer number n_0 of time samples:

$$\mathbf{x}(n) = d(n - n_0) \tag{25}$$

If the input $d(n)$ is a weakly stationary stochastic process, and we assume that the filter coverges, an estimate of the RFI signal is computed by the filter:

$$\rho(n) \approx \mathbf{w}^T(n)\mathbf{x}(n) \tag{26}$$

The radar signal plus thermal noise can thus be approximated by:

$$s(n) + v(n) \approx d(n) - \rho(n) = d(n) - \mathbf{w}^T(n)\mathbf{x}(n) \tag{27}$$

In the paper referenced, $0 < \beta < 2$, and for their tests they used $\beta = 0.015$, $n_0 = 1$ and a filter length of order 256.

2.8 SAR imaging

When the RAW radar data has been appropriately pre-processed, a time- or frequency domain SAR imaging algorithm is employed to transform the 2D radar image to a 2D normal image. Time-domain algorithms are presented here.

2.8.1 Global Backprojection

Global Backprojection is a time-domain algorithm for forming the 2D image from the radar data. It is the baseline on which comparisons with new time-domain algorithms is made. The algorithm is described by a single equation [10]:

$$h(x, \rho) = \int_{\frac{-L}{2}}^{\frac{L}{2}} g(x', r)\, dx' \tag{28}$$

In the above equation, $h(x, \rho)$ is the image pixel value at position x in cross-range and ρ in range. When the flight track is straight, the following relation holds:

$$r = \sqrt{(x' - x)^2 + \rho^2} \tag{29}$$

We thus get:

$$h(x,\rho) = \int_{\frac{-L}{2}}^{\frac{L}{2}} g(x', \sqrt{(x'-x)^2+\rho^2})\, dx' \tag{30}$$

When this is implemented on a computer, the above summation is discrete, and the number of summations depends on the number of aperture slices in the radar data. The number of operations to form an image with GBP is proportional to $O(N_x N_\rho N_{slices})$.
Writing GBP in discrete form gives us:

$$\mathbf{h}[x,\rho] = \sum_{x'=1}^{N_{slices}} \mathbf{g}[x', \sqrt{(x'-x)^2+\rho^2}]\ , x', x, \rho \in Z \tag{31}$$

The main advantage of GBP lies in its simplicity, and applicability to images of unlimited size, limited only by the computer processing time and memory requirements.

2.8.2 Local Backprojection

Local Backprojection is a two-stage algorithm based on GBP, which reduces the computational load. The extra step in LBP is called beamforming. The algorithm works by forming the images for the different subapertures independently, and then all subimages are combined to form the final image [10]. The computational load for LBP is given by $N_{op} \approx N_a \left(\frac{N_x N_\rho}{N_{a,sa}}\right)$, where N_a is the number of aperture positions and $N_{a,sa}$ is the number of subaperture positions. The computational load for LBP is thus a factor of $N_{a,sa}$ lower than GBP. The LBP algorithm is defined as follows:

$$h(x,\rho) = \sum_{m=1}^{M} \int_{x_m-\frac{L_s}{2}}^{x_m+\frac{L_s}{2}} g\left(x', \sqrt{(x_c-x_m)^2+\rho_c^2} + \frac{\{(x'-x_m)-(x-x_c)\}(x_m-x_c)+(\rho-\rho_c)\rho_c}{\sqrt{(x_c-x_m)^2+\rho_c^2}}\right)\, dx' \tag{32}$$

Here, x_m is the center pixel of the m:th subaperture, and (x_c, ρ_c) is the center coordinates of a subimage.
Again writing this in discrete form gives us:

$$\mathbf{h}[x,\rho] = \sum_{m=1}^{M} \sum_{n=x_m-N/2}^{x_m+N/2} \mathbf{g}\left[x', \sqrt{(x_c-x_m)^2+\rho_c^2} + \frac{\{(x'-x_m)-(x-x_c)\}(x_m-x_c)+(\rho-\rho_c)\rho_c}{\sqrt{(x_c-x_m)^2+\rho_c^2}}\right] \tag{33}$$

The inner integral (summation) is called the subaperture beam.

2.9 SAR image apodization

The reflected signal from a target has a main lobe and sidelobes. If a weakly reflecting object is located in close proximity to an object which reflects strongly, the sidelobes from the strong reflector may be greater than the main lobe of the weak reflector. This means that the object with greater reflection may shadow the smaller object, which is undesirable. The method to compensate for this effect is known as *apodization*, in which the sidelobes are suppressed with appropriate filtering. In [12], separable and non-separable windowing functions are evaluated. A separable window in 2D frequency space is generally given by:

$$W_{sep}(k_x, k_y) = W_{k_x}\left(\frac{k_x}{2k_c \sin\frac{\phi_o}{2}}\right) W_{k_y}\left(\frac{k_y - k_c}{k_{max} - k_{min}}\right) \tag{34}$$

Here, k_x, k_y, k_c are the wavenumbers in crossrange, range and center wavenumber of the radar signal, and ϕ_0 is the integration angle. k_{max}, k_{min} are the max and min wavenumbers of the signal. In the paper, a non-separable window is described by:

$$W_{non-sep}(k_x, k_y) = W_{\phi}\left(\frac{tan^{-1}\left(\frac{k_x}{k_y}\right)}{\frac{\phi_0}{2}}\right) W_{k_r}\left(\frac{\sqrt{k_x^2 + k_y^2} - k_c}{k_{max} - k_{min}}\right) \tag{35}$$

Here, k_r is the range wavenumber in the frequency domain.
The authors in the paper cited compared the two windows using both Bartlett and Hamming windows. The difference between separable and non-separable windows was shown to be small for SAR systems with small fractional bandwidth and small integration angles. However, for systems employing large fractional bandwidths and larger integration angles, non-separable windows suppressed non-orthogonal considerably more than a separable window.
It should be noted that other window functions may be used

2.10 Related work

In [4], a through-wall SAR system is used in conjunction with contourlet domain hidden Markov tree based detection to automatically detect targets located inside and beyond walls. The results are of modest quality, and much more work is needed, since the processed images are of low quality.

No other research using SAR at close range to scan through walls has been found.

Related to computational complexity, the authors in [5] implemented the direct filtered backprojection algorithm on a graphics processing unit using CUDA, and achieved a processing speedup of up to 60 times compared to the computational time of the CPU.

2.11 Sources of RF interference

Since the radar equipment operates in the public UHF and SHF bands, we must consider possible sources of interference. In Sweden, *Post och Telestyrelsen* manages the frequency spectrum, and gives a list of frequency allocations within Sweden. The complete spectrum is located in the appendix.
From the extensive table, we see that the spectrum is filled with services in the frequency band under study (approximately UHF). However, most allocations in the upper bands are dedicated to GPS or other positioning services. In addition to these, frequencies have been allocated to the Onsala space observatory. Neither of these services should a priori pose any threat to the radar imagery. What is more unnerving is that both 2G, 3G and wireless local area networks are located in this large frequency band, and since all three are in frequent use today, they may need to be filtered out from the radar image before SAR imaging.

3 System description

3.1 System requirements

To fully simulate the scanning scenario, the model must take antenna beamwidth, antenna elevation and radar tilt into account, as well as the waveform. Chirp signals are the de-facto standard in long-range SAR systems utilizing a high fractional bandwidth, and as such we use a chirp waveform with customizable start frequency and bandwidth in the simulation model. Even though the radar system used is not configured to emit a chirp waveform, we use it in the model for its sheer simplicity. The model must in addition calculate the fractional area exposed by the radar as it moves throughout the image to generate realistic raw radar data.

3.2 System model and design

To be able to say with a certain probability that a system works in real life, one should test the system with control data. The control data must be deterministic, or at least be of such a nature that one knows how the system will respond to the control data. If the system produces correct output from the control data, one can be certain that the system works, and the system can be used with real data.

To be able to have any confidence in the SAR algorithms and processing developed during this thesis, a radar simulation model had to be developed. The purpose of the simulation model was to simulate radar data, that is the raw radar data as it is received from a radar. To achieve this, one must specify the scene geometry, where scattering objects are located, the waveform characteristics, platform altitude and antenna beamwidth.

3.3 Implementation of system model

The simulation model developed in this thesis consists of a number of steps, where the user first specifies the scene geometry and where scattering objects are located. The output is a matrix containing ones at scatterer positions. Once the scene has been created, the user specifies start frequency and bandwidth of the chirp waveform used in the radar. This effectively inserts the waveform at the positions where scattering objects are located in the scene.

The raw radar data is generated by taking the antenna beamwidth into account, which means that radar data from several crossrange bins are projected onto one column. The range in a certain column is calculated by simple trigonometry:

$$R = \sqrt{(C_r - c)^2 + r^2} \tag{36}$$

Here, C_r is the crossrange bin over which the antenna beam illuminates, c is the column being calculated and r is the row in the crossrange bin being calculated. For a point scatterer in the middle of the scene, this effectively

generates a hyperbola in radar image space. Scilab and C code is located in the appendix.
Once the raw data has been generated, the raw data matrix is pulse compressed with a time-reversed and conjugated version of the chirp signal. The pulse compression is implemented in the frequency domain by employing zero padding and the FFT algorithm.
The final step is to employ a SAR imaging algorithm to de-skew the hyperbola into its correct position in real image space. In the simulation GBP has been used for simplicity (Eq. 28). As can be seen in the figure, GBP correctly focuses most of the radar power in the correct position at the center of the image. The exact thape of all three figures depends on the resolution of the scene and the waveform used.

3.4 Verification of system model

To verify both Scilab and C models, a start frequency of 900MHz and bandwidth of 4.1GHz was used in conjunction with various TBP to generate the chirp signal. The chirp was inserted in the center of a rectangular image matrix. The radar imaging algorithm was applied to the image matrix, upon which a radar "distorted" image was generated. The radar image was then pulse-compressed, and finally GBP was employed. This generates in total four radar images, the last being a 2D FFT of the SAR image after GBP. By varying the TBP, one can vary the spread of the fan-shape in 2D SAR frequency image space, which is equivalet to varying target resolution in SAR image space. A wider fan shape in 2D frequency space indicates coarser resolution, whilst a narrower fan shape is equivalent to finer target resolution.

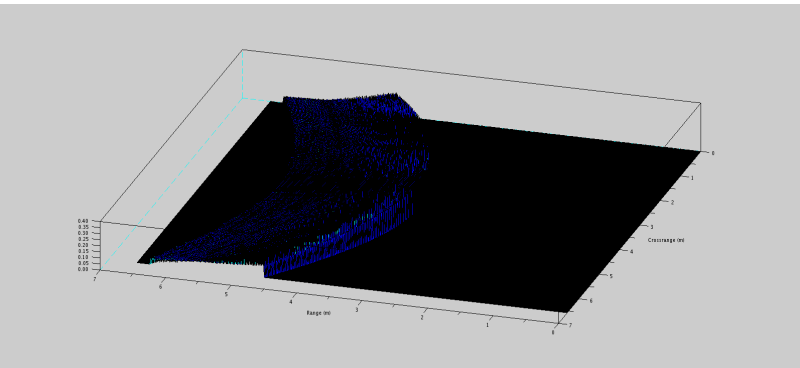

Figure 9: Simulated radar image with TBP 30 and azimuth beamwidth 80 degrees

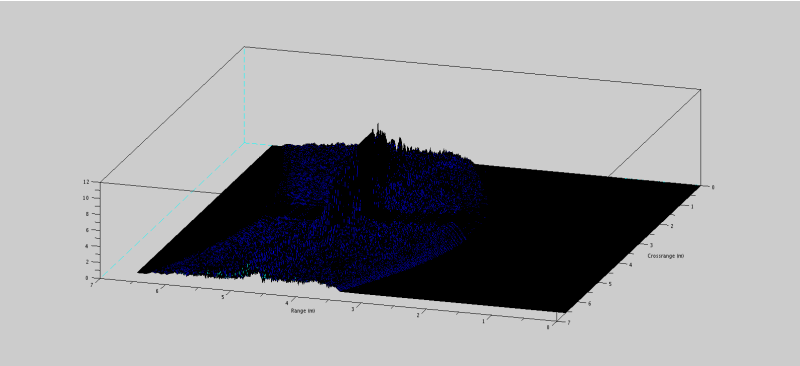

Figure 10: Pulse-compressed radar image with TBP 30 and azimuth beamwidth 80 degrees

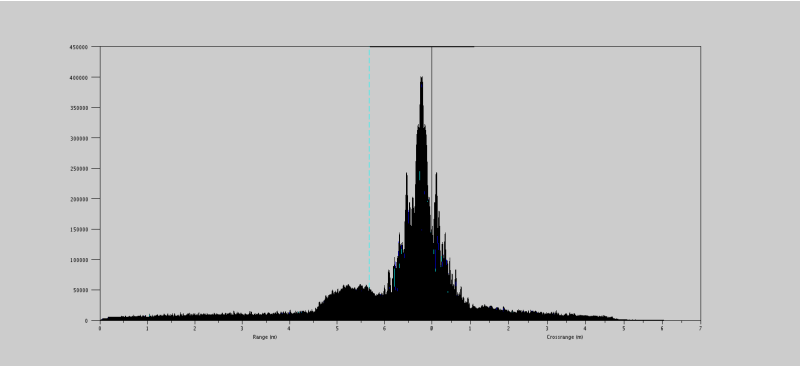

Figure 11: GBP image of pulse-compressed image with TBP 30 and azimuth beamwidth 80 degrees

3.5 Hardware description

The hardware used to gather real radar data consisted of a Novelda Impulse Radar in a bistatic setup. In addition to the radar chip, the system uses an Atmel AT91SAM7 microcontroller for communication between radar chip and computer. The Novelda Impulse Radar uses a staggered PRF system with 512 samplers operating as a number of radars in parallel. The radar sampling frame span can be adjusted, which enables selection of the unambiguous range. The radar system uses Vivaldi antennas from Imego [1] operating from 900 MHz to 5 GHz and has -3dB beamwidths of 40 and 100 degrees in azimuth and elevation, respectively. Another antenna previously used for measuring snow depth with radar is used, and operates within 3.1-5.6 GHz with a beamwidth of 60 degrees in both azimuth and elevation.

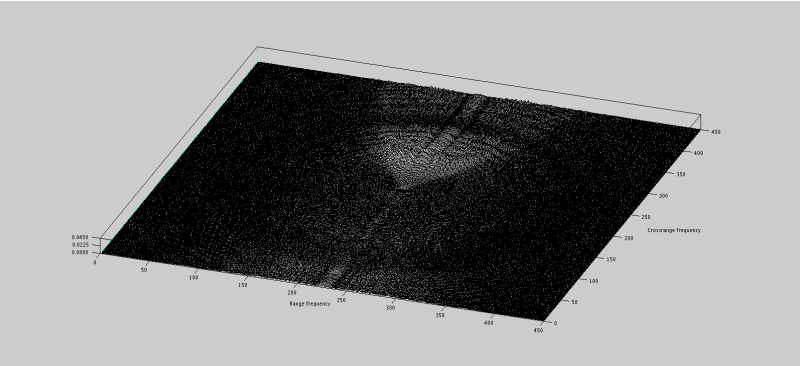

Figure 12: 2D FFT of GBP image with TBP 30 and azimuth beamwidth 80 degrees

3.5.1 Antenna far-field calculation

When using any radiating equipment, it is useful to know where the antenna far-field begins. If the antenna is used on distances shorter than the far-field range, the antenna will couple to the object inside its reactive region, which is unsuitable because the spherical propagation model breaks down at the boundary. The far-field region begins where the phase error is at a maximum of $\frac{1}{16}$ of a wavelength. The following relation describes this distance:

$$R_{far-field} = \frac{2D^2}{\lambda} \tag{37}$$

Here, D is the largest linear dimension of the antenna. For the Vivaldi [1] antenna, this is 150mm. The shortest and longest wavelengths are 6 and 33cm, respectively. This gives us:

$$\frac{2 * 0.15^2}{0.06} \approx 0.75 \ [m] \tag{38}$$

$$\frac{2 * 0.15^2}{0.33} \approx 0.136 \ [m] \tag{39}$$

This means that when designing measurement scenarios, they must be performed at least 0.75 m from the target with the Vivaldi antenna.

For the snow radar, the largest linear dimension is 34.4mm. The shortest and longest wavelengths are 5.35 and 9.67 cm, which gives us far-field distances of:

$$\frac{2 * 0.0344^2}{0.0967} \approx 2.45 \ [cm] \tag{40}$$

$$\frac{2 * 0.0344^2}{0.0535} \approx 4.42 \ [cm] \tag{41}$$

4 Problem solution

4.1 Test scenarios

To be able to evaluate processing algorithms on real radar data, a number of scanning scenarios had to be developed. These vary from simple to more complex set ups, with varying amounts of objects, wall depths and wall materials.

4.1.1 Test case α

To test the most basic functionality of the radar equipment, the simplest scenario is used, in which a scattering object is raised above ground on a narrow platform.

4.1.2 Test case β

Being able to evaluate the radar image due to a wall in itself gives insight into how more complex radar images should be processed, and as such this scenario simply scans a flat wall.

4.1.3 Test case γ

This scenario places an object in front of a flat wall. The purpose is to evaluate the radar image generated when a flat object (a wall) is located behind an object.

4.1.4 Test case δ

This scenario is a mirror of test case γ, with the difference being that the radar scans the blocking side of the wall, with the scatterer being located behind the wall.

4.2 Creating a matched signal wavform for pulse compression

4.3 Applying digital filters

4.4 Generating an image

4.5 Specifying parameter requirements

5 Real-time implementation

5.1 Verification of implementation

6 Managing fuzzy scanning

To enable a user more freedom in scanning a surface, the radar echoes must be aligned based on the movement of the handheld radar. In this section I present a detailed analysis of how such a system can be built, what components are required and the algorithms needed to align the radar data.

7 Results

8 Future work

A Radio frequency spectrum in Sweden

Table 1:

Fr.o.m MHz	T.o.m MHz	Duplexband	Anvndning
880	915	925 - 960	GSM & UMTS
916	921	871 - 876	TRA-ECS
921	925	876 - 880	GSM-R
925	960	880 - 915	GSM & UMTS
960	1164		Luftfartsradio (DME)
1026	1034	1086 - 1094	Luftfartsradio (SSR)
1086	1094	1026 - 1034	Luftfartsradio (SSR)
1164	1215		GALILEO
1164	1215		Luftfartsradio (DME)
1215	1240		Radiolokalisering
1215	1237		GPS
1215	1240		Radionavigering fr luftfart
1237	1260		GLONASS
1240	1300		Radionavigering fr luftfart
1240	1300		Amatrradio
1260	1300		GALILEO
1300	1350		Militr anvndning
1300	1350		Radionavigering fr luftfart
1300	1350		Radiolokalisering
1330	1400		Radioastronomi Onsala
1350	1375		Militr anvndning
1350	1355		Radiolokalisering
1375	1400	1427 - 1452	Fast radio punkt till punkt
1400	1427		Radioastronomi Onsala
1427	1452	1375 - 1400	Fast radio punkt till punkt
1452	1479.5		Rundradio (T-DAB)
1479.5	1492		Ljudrundradio satellit
1492	1518		Militr anvndning
1518	1525		Militr anvndning
1518	1525		Satellit
1525	1559		Satellit
1525	1530		Militr anvndning
1525	1559		Satellit
1530	1535		Militr anvndning
1535	1544		Militr anvndning
1544	1545		Sjfartsradio
1545	1559		Militr anvndning
1559	1591		GALILEO
1563	1587		GPS
1591	1610		GLONASS
1610	1626.5		Jordstationer (mobila satellitsystem)

Table 2:

1610.6	1613.8		Radioastronomi Onsala
1613.8	1626.5		Jordstationer (mobila satellitsystem)
1626.5	1645.5		Jordstationer (mobila satellitsystem)
1645.5	1646.5		Sjfartsradio
1646.5	1660.5		Jordstationer (mobila satellitsystem)
1660	1670		Radioastronomi Onsala
1668	1670		Jordstationer (mobila satellitsystem)
1670	1675		Jordstationer (mobila satellitsystem)
1675	1690		Meteorologi via satellit
1690	1700		Meteorologi via satellit
1700	1710		Meteorologi via satellit
1710	1785	1805 - 1880	GSM & UMTS
1718.8	1722.2		Radioastronomi Onsala
1785	1805		vrigt
1805	1880	1710 - 1785	GSM & UMTS
1880	1900		DECT
1900	1920		UMTS
1920	1980	2110 - 2170	UMTS
1920	1980	2110 - 2170	UMTS
1980	2010	2170 - 2200	Jordstationer (mobila satellitsystem)
2010	2025		UMTS
2025	2110		Militr anvndning
2025	2110	2200 - 2290	Rymdfarkostkontroll
2110	2170	1920 - 1980	UMTS
2170	2200	1980 - 2010	Satellit
2200	2290		Militr anvndning
2200	2290	2025 - 2110	Rymdfarkostkontroll
2290	2300		Militr anvndning
2300	2450		Landmobil radio
2300	2450		Amatrradio
2400	2483.5		Dataverfring trdlsa ntverk
2400	2483.5		Allmn kortdistansradio ISM
2400	2450		Militr anvndning
2400	2483.5		Allmn kortdistansradio ISM
2446	2454		RFID
2450	2483.5		Militr anvndning
2450	2483.5		Landmobil radio
2483.5	2500		Satellit
2500	2690		TRA-ECS
2690	2700		Radioastronomi Onsala

Table 3:

2700	2900		Radionavigering fr luftfart
2900	3100		Radionavigering fr sjfart
2900	3100		Sjfartsradar
2900	3100		Militr anvndning
3100	3300		Radiolokalisering
3100	3300		Militr anvndning
3260	3267		Radioastronomi Onsala
3300	3400		Radiolokalisering
3300	3400		Militr anvndning
3332	3339		Radioastronomi Onsala
3345.8	3352.5		Radioastronomi Onsala
3400	3600		TRA-ECS
3600	3800		TRA-ECS
3800	4200		Satellit
3900	4200		Militr anvndning
4200	4400		Radionavigering fr luftfart
4400	4500		Militr anvndning
4500	4800		Militr anvndning
4500	4800	6725 - 7075	
4800	4990		Militr anvndning
4825	4835		Radioastronomi Onsala
4950	4990		Radioastronomi Onsala
4990	5000		Radioastronomi Onsala
5000	5150		Radionavigering fr luftfart
5000	5150		Radionavigering fr luftfart
5000	5150		Radionavigering fr luftfart
5091	5150		Radionavigering fr luftfart
5150	5250		Luftfartsradio (telemetri)
5150	5250		Radionavigering fr luftfart
5150	5250		Dataverfring Trdlsa ntverk
5250	5350		Dataverfring Trdlsa ntverk
5250	5255		Militr anvndning
5250	5350		Kortdistansradio (SRD)
5255	5350		Militr anvndning
5350	5460		Militr anvndning
5440	5440		Radionavigering fr luftfart
5460	5470		Radionavigering fr luftfart
5460	5470		Militr anvndning
5470	5725		Dataverfring Trdlsa ntverk
5470	5650		Radionavigering fr sjfart
5470	5570		Militr anvndning
5470	5725		Dataverfring Trdlsa ntverk
5525	5525		Radionavigering fr luftfart
5570	5650		Militr anvndning

B Matlab and Scilab source code

C Real-time implementation source code

References

[1] http://www.imego.com/research-and-development/electromagnetic-sensors-and-systems/industrial-solutions/ultra-wideband-radar.aspx.

[2] Ahmed, I. *Study of the Local Backprojection Algorithm for Image Formation in Ultra Wideband Synthetic Aperture Radar.* Blekinge Institute of Technology Doctoral Dissertation Series, 2008.

[3] Anthony Freeman, B. C. A uhf sar mission to mars (2003).

[4] Chan, B. Contourlet domain hidden markov tree based detection algorithm for drdc through-wall sar (twsar) system applications. vol. 7699 (Orlando, FL, United states, 2010), The Society of Photo–Optical Instrumentation Engineers (SPIE) –.

[5] Fasih, A., and Hartley, T. Gpu-accelerated synthetic aperture radar backprojection in cuda (2010). 1408 – 13.

[6] Fransson, J. E., Walter, F., Blennow, K., Gustavsson, A., and Ulander, L. M. Detection of storm-damaged forested areas using airborne carabas-ii vhf sar image data. *IEEE Transactions on Geoscience and Remote Sensing 40*, 10 (2002), 2170 – 2175.

[7] Guarnieri, M. The early history of radar. *IEEE Industrial Electronics Magazine 4*, 3 (Sept. 2010), 36 – 42.

[8] Hülsmeyer, C. Verfahren, um entfernte metallische gegenstände mittels elektrischer wellen einem beobachter zu melden. *Kaiserliches Patentamt, Patent nr 165546*, DE 165546 (1904).

[9] Liu, S., Hanssen, R., and Mika, A. On the value of high-resolution weather models for atmospheric mitigation in sar interferometry. vol. 2 (Cape Town, South africa, 2009), II749 – II752.

[10] Pettersson, M. Detection of moving targets in wideband sar. *Aerospace and Electronic Systems, IEEE Transactions on 40*, 3 (july 2004), 780 – 796.

[11] Scilab Consortium. *Scilab: The free software for numerical computation.* Scilab Consortium, Digiteo, Paris, France, 2011.

[12] Sjogren, T. K., Vu, V. T., and Pettersson, M. I. 2d apodization in uwb sar using linear filtering (Vancouver, BC, Canada, 2011). 1689 – 1692.

[13] Sjgren, T. *Development and evaluation of SAR algorithms for image formation and speed estimation in wideband SAR.* Blekinge Institute of Technology Licentiate Dissertation Series, 2010.

[14] Skolnik, M. I. *Radar Handbook*, 3 ed. McGraw-Hill Professional, 2009.

[15] Vu, V. T. *Ultrawideband-Ultrawidebeam Synthetic Aperture Radar Signal Processing and Applications*, 13 ed. Blekinge Institute of Technology Doctoral Dissertation Series, 2011.

[16] Vu, V. T., Sjogren, T. K., and Pettersson, M. I. A comparison between fast factorized backprojection and frequency-domain algorithms in uwb lowfrequency sar. vol. 4 (Boston, MA, United states, 2008), IV1284 – IV1287.

[17] Vu, V. T., Sjogren, T. K., Pettersson, M. I., and Gustavsson, A. Definition on sar image quality measurements for uwb sar. vol. 7109 (Cardiff, Wales, United kingdom, 2008), SPIE Europe.

[18] Vu, V. T., Sjogren, T. K., Pettersson, M. I., Hakansson, L., Gustavsson, A., and Ulander, L. M. H. Rfi suppression in ultrawideband sar using an adaptive line enhancer. *IEEE Geoscience and Remote Sensing Letters 7*, 4 (2010), 694 – 698.

[19] Vu, V. T., Sjogren, T. K., Pettersson, M. I., and Hakasson, L. An approach to suppress rfi in ultrawideband low frequency sar (Washington DC, United states, 2010). 1381 – 1385.